Self-Stability and Induced-Stability Analysis for Frequency and Voltage in Grid-Forming VSG System With Generic Magnitude–Phase Model

Li, Chang; Li, Yong; Du, Yan; Gao, Xingle; Yang, Yaqian; Cao, Yijia; Blaabjerg, Frede

Published in:
IEEE Transactions on Industrial Informatics

DOI (link to publication from Publisher):
10.1109/TII.2024.3418008

Publication date:
2024

Document Version
Accepted author manuscript, peer reviewed version

Self-Stability and Induced-Stability Analysis for Frequency and Voltage in Grid-Forming VSG System with Generic Magnitude-Phase Model

Chang Li, Yong Li, *Senior Member, IEEE*, Yan Du, Xingle Gao, Yaqian Yang, Yijia Cao, *Fellow, IEEE* and Frede Blaabjerg, *Fellow, IEEE*

***Abstract*—Frequency and voltage stability of grid-forming virtual synchronous generator (GFM-VSG) grid-tied system becomes significant in inertia and damping support when GFM-VSG is attached to power network. This research proposes a generic Open-Loop System Model (OLSM) for the frequency-voltage induced-stability analysis, where the dynamics of rate of change of frequency (RoCoF) is a dynamic process that acts on rate of change of voltage (RoCoV) and then in turn reacts on RoCoF. In addition, frequency self-stability is evaluated by magnitude-phase feedback analytical model (MPFAM), where the frequency dynamics are identified by interaction between RoCoF and frequency bias (FB). Also, it is found that inertia is origin of occurrence of low-frequency oscillation (LFO), which induces a natural phase bias between RoCoF and FB. It is found that GFM-VSG can operate stably in weak grid but cannot operate well in ultra-strong grid condition. Finally, theoretical analysis is validated by simulations and experiments.**

***Index Terms*—grid-forming virtual synchronous generator (GFM-VSG), low-frequency oscillation (LFO), Open-Loop System Model (OLSM), magnitude-phase feedback analytical model (MPFAM), induced-stability**

I. Introduction

TO build up new type of power system with renewable energy as the main part becomes an important approach to achieve the 'dual carbon goal', i.e., Peak carbon dioxide emissions and carbon neutrality. Nevertheless, intermittency caused by renewable energy as well as low-inertia and poor-damping property originated from power electronics converter (PEC) inevitably triggers a series of stability issues [1]. This series of instability aggravate secure operation of power grid which cannot provide reliable and high-quality power to the city loads.

To overcome instability issues caused by low-inertia and poor-damping property, virtual synchronous generator (VSG) control technique [2]-[16] has been emerging to enhance inertia and damping of the system by emulating dynamic property of synchronous generator (SG). However, the prerequisite of making good use of VSG is that it can maintain stable and synchronize with power grid in a grid-friendly manner. Thus, stability of grid-interface with VSG becomes significant for the reliable and high-quality inertia and damping support.

Prior researches on topics of frequency and voltage stability in VSG are mainly focused on various stability analysis and modeling methods, e.g., state-space model [2]-[8], impedance model [9]-[11], magnitude-phase motion equation (MPME) model [12]-[14]. By means of those methods, stability of GFM-VSG can be viewed from different perspectives.

For an example, the state-space model was established to develop eigenvalue analysis and a state feedback controller was proposed to improve robust stability of single-VSG-infinite-bus system [2]. In addition, the impact of virtual inertia and virtual damping factor on rate of change of frequency (RoCoF) and frequency bias (FB) was studied. Furthermore, the impact of VSG on low-frequency oscillation (LFO), angular stability, and frequency stability was investigated in various grid operation conditions by the state-space model using eigenvalue analysis [3]-[8]. And participation factor analysis was developed to identify different oscillatory modes.

Impedance model can observe the terminal port characteristics of the GFM-VSG system and thus identify stability. As an example, a sequence impedance model was established to develop stability analysis by means of Generalized Nyquist Stability Criterion [9]. Besides of this, a sequence impedance model was proposed to study the frequency resonance issue at the synchronous frequency for GFM-VSG system [10]. But it was lack of cognition to the physical significance of loss of stability in GFM-VSG system. In addition, a small-signal impedance model was established to explore frequency stability of GFM-VSG system and the conclusion was drawn that the GFM-VSG system will be unstable as long as grid impedance is large enough [11].

MPME model was developed to observe frequency stability of GFM-VSG system by identifying the damping-torque and synchronizing-torque at the dominant frequency [12]-[14]. In

Manuscript received on 13th September, 2023, and revised on 19th March, 2024 and 28th May, 2024, and accepted on 16th June, 2024. This work was supported by the State Grid Corporation Headquarters Management Technology Project: Operation Characteristics and Stability Control of Universal Active Support Power Electronic Equipment Power System (52120522003P). Corresponding author: (*Yong Li*, yongli@hnu.edu.cn) Yong Li is Corresponding author

Chang Li is with the College of Electrical and Automation Engineering and Anhui Province Key Laboratory of Renewable Energy Utilization and Energy Saving, Hefei University of Technology, Hefei 230009, China (e-mail: changli@hnu.edu.cn).

Yong Li and Yijia Cao are with the College of Electrical and Information Engineering, Hunan University, Changsha 410082, China.

Yan Du is with the College of Electrical and Automation Engineering, Hefei University of Technology, Hefei 230009, China.

Xingle Gao is with Economic Research Institute of State Grid Hebei Electric Power Co., Ltd, Shijiazhuang, China (xinglegao@hnu.edu.cn)

Yaqian Yang is with the School of Engineering, Anhui Agricultural University, Hefei 230009, China (yaqianyang@ahau.edu.cn)

Frede Blaabjerg is with the Department of Energy Technology, Aalborg University, 9220, Aalborg, Denmark. (fbl@energy.aau.dk)

[12], a generalized stabilizer-oriented design method was proposed to guarantee that GFM-VSG system can operate in stable region. In addition, the stable region was determined by the proposed magnitude-phase feedback analytical method. Besides of this, MPME model was proposed to assess frequency stability of GFM-VSG system through positive/negative of damping/synchronizing torque [13]. However, one disadvantage of MPME model was that virtual inertia part was not included in the torque analysis, which was filled up by [14]. In [14], a feedback model was proposed to include inertia, damping and stiffness to analyze dynamic behavior between RoCoF and FB. Absolutely, researches of small-signal stability on topics of VSG can be also classified from perspective of state-variable, i.e., frequency stability [2]-[5], [7]-[8] voltage stability [2], [9]-[12], [15] and angle stability [6], [14]. This classification can be found in definition and classification of power system stability [17]. However, it was a little bit different from the stability definition of microgrids[16].

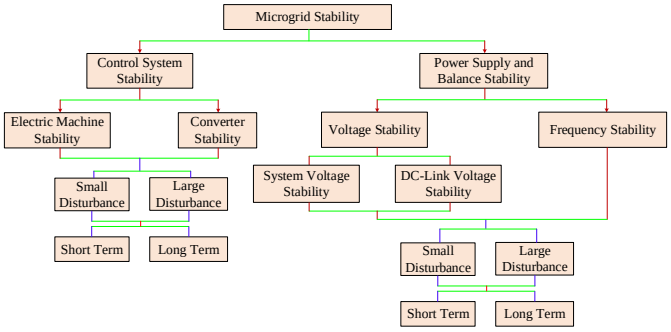

Fig. 1 Classification of stability in Microgrids [16]

The main differences lie in that system AC voltage stability can be classified into small- and large-disturbance including short- and long-term, which is more generalized than voltage stability classification in [17]. But the microgrid stability definition [16] was lack of small disturbance synchronous stability and large perturbation transient angle stability as well as oscillation propagation mechanism between frequency and voltage. And the mechanism of small signal synchronous stability and oscillation propagation will be researched in this work.

TABLE I. COMPARISON AMONG THE GENERIC OLSM AND MPFAM, EIGENVALUE ANALYSIS WITH STATE SPACE MODEL, GENERALIZED NYQUIST CRITERION AND MPME MODEL

Model / Attribute	Eigenvalues analysis with state space model	Generalized Nyquist Stability Criterion with impedance ratio	MPME Model	Generic OLSM and MPFAM
Oscillation frequency and damping	Can judge	Cannot judge	Conditionally judge	Conditionally judge
Qualitative Stability	Can judge	Can judge	Can judge	Can judge
Quantitative Stability Margin	Can judge	Can judge	Cannot intuitively judge	Can judge
Synchronism	Can judge	Cannot judge	Can judge	Can judge
Induced-stability and self-stability	Cannot judge	Cannot judge	Cannot judge	Can judge
Oscillation propagation mechanism	Cannot judge	Cannot judge	Cannot judge	Can judge
Interactive behavior between RoCoF and FD	Cannot judge	Cannot judge	Cannot judge	Can judge
Terminal characteristics of impedance	Cannot judge	Can judge	Cannot judge	Cannot judge

Basing on definition and classification framework in Fig. 1, this research proposes a new generic modeling method to identify the frequency and voltage stability as well as the oscillation propagation. Mechanism in frequency and voltage in GFM-VSG system is discussed from perspectives of self-stability and induced-stability. The framework of self- and induced-stability are identified by the unified modeling method including Open-Loop System Model (OLSM) and Magnitude-Phase Feedback Analytical Model (MPFAM). It is stressed that these two models cannot be separately seen and is unified basing on the duality principle and dialectics. Especially the induced-stability reflected by the ***oscillation propagation*** can be clarified by the unified model which combines OLSM and MPFAM. The comparison Table I highlights the innovations and contributions of this work. It can be seen that the proposed generic OLSM and MPFAM have most of the attributes and advantages over traditional methods especially have the unique attribute of induced- and self-stability as well as oscillation propagation mechanism. And this paper develops the continuous research on [15] to expand dynamic analysis in GFM-VSG grid-tied system. The major contributions of this work are summarized as follows:

1) This research proposes a generic Open-Loop System Model (OLSM) to identify the motion trajectory of RoCoF/RoCoV and FB and thus evaluating frequency/voltage induced-stability. The proposed OLSM is distinguished from conventional Open-Loop transfer function that develops stability analysis by seeing magnitude margin and phase margin. Instead, it can quantitatively evaluate the dynamic coupling between frequency and voltage magnitude as well as oscillation propagation. The OLSM provides a perspective to identify the oscillation transferring between the frequency and voltage magnitude as well as mechanism of loss of synchronism (LoS).
2) The generic model, i.e., OLSM combined with MPFAM, can universally clarify the mechanism of both self-stability and induced-stability, where duality principle and symmetry characteristics can be found in the systematic generic model. Under the modeling framework with feedback analytical method, it is found that GFM-VSG can operate stably in weak power network but cannot operate well in ultra-strong power network. Besides, it has a risk of LoS in the weaker grid condition but this condition can be avoided during the stage of grid-planning or grid-dispatching. This characteristic provides foundation for future exploration of the safety and stable regions of the GFM-VSG system.
3) It is found that the origin of the oscillation is that damping

of the system is not matched with the virtual inertia and stiffness provided by power network. Damping is not the unique factor to influence the oscillation. Although damping can mitigate oscillation, but the inertia always leave the state variables maintaining 'original state', which will result in mismatch between inertia, damping and stiffness. This mismatch cause that RoCoF cannot synchronize with FB.

4) It is found that grid strength not only impacts the damping performance and critical oscillation frequency but also influence the synchronous stability of the system. The system has a higher risk of LFO when VSG is attached to stronger grid strength power network while the system has a higher risk of LoS when VSG is connected to weaker grid strength power network. This finding can help to guide the controller parameterization optimization and design.

5) It is found that In fact, the extent of the 'weak' with weak grid is comparatively/relatively where there is no strict and absolute boundary between weak- and ultra-weak-grid. From another dimension, the 'weak' also means that the VSG in grid-forming mode can operate more stably and provide better frequency and voltage support capability than that in grid-following mode.

The remainders of this research are summarized as follows. In the next Section, a physical OLSM is established to analyze the induced-stability and oscillation propagation in GFM-VSG system. And MPFAM is presented to study self-stability of GFM-VSG system. In Section III, stability analysis is developed to illustrate the effectiveness of the proposed model and elaborate the physical mechanism of LFO and synchronous stability of the system. Besides, the mechanism of LFO is interpreted from perspective of inertia-damping-stiffness matching. Simulations and experiments are carried out in Section IV. Section V finally draws the conclusion.

II. Physical Model and Analytical Method

In this section, the physical model and analytical method are proposed for mechanism clarification of self-stability and induced-stability as well as the oscillation propagation.

A. Small signal model of grid-forming VSG system

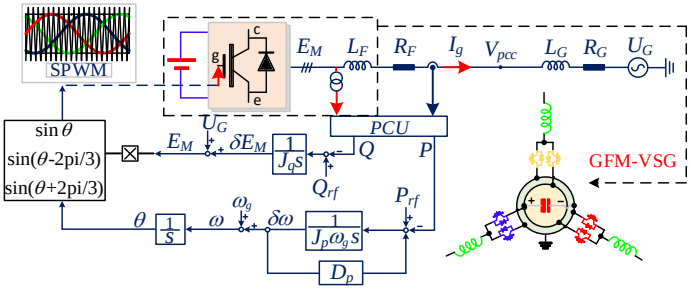

Fig. 2 Topology and control strategy of grid-forming VSG (GFM-VSG) system

The stiff DC voltage source is connected on DC-side of VSG and feed the power to AC power network via VSG and distribution line. PCU is the abbreviation of 'power collection unit'. The swing equation of VSG control is expressed as [14]:

$$\begin{cases} 2\pi J_p \omega_g \frac{df}{dt} + 2\pi D_p \delta f = P_{rf} - P \\ J_q \frac{dE_M}{dt} = Q_{rf} - Q \end{cases} \tag{1}$$

where J_p, D_p denote the virtual inertia and virtual damping factor of active-power channel, J_q signifies virtual inertia factor of reactive-power channel. δf is the frequency *bias* (FB) between VSG and power network, and f is the frequency of VSG. E_M is the magnitude of output voltage of VSG, Q_{rf} and Q represent the reference and real reactive-power. P_{rf} and P denote the reference and real active-power.

Moreover, the circuit equation of the VSG system can be derived in *dq*-coordinate according to Fig. 2 [12], i.e.,

$$\begin{cases} E_M \cos\delta\theta - U_G = I_g cos\delta\varphi_i (sL + R) - I_g sin\delta\varphi_i \omega_0 L \\ E_M \sin\delta\theta = I_g sin\delta\varphi_i (sL + R) + I_g cos\delta\varphi_i \omega_0 L \end{cases} \tag{2}$$

where U_G and I_g are the grid voltage and grid-integrated current, 'δ' means the bias between the VSG angle and the grid angle. It was because all of the sinusoidal voltages and currents are transformed into the synchronous reference frame (SRF) tracking synchronously with power network, and all of the fundamental-frequency rotating components of the angle (i.e., ωt) are removed. R and L denote total resistance and inductance, i.e., R=R_F+R_G, L=L_F+L_G.

In addition, active- and reactive-power can be expressed as the function of output phase angle and output voltage magnitude of VSG [12], i.e.,

$$\begin{cases} P = Re\left[\dot{E_M} I_g^*\right] = E_M \cos\delta\theta I_g cos\delta\varphi_i + E_M \sin\delta\theta I_g sin\delta\varphi_i \\ Q = Im\left[\dot{E_M} I_g^*\right] = E_M \sin\delta\theta I_g cos\delta\varphi_i - E_M \cos\delta\theta I_g sin\delta\varphi_i \end{cases} \tag{3}$$

By developing Laplace Transformation of (1), the swing equation in *s*-domain can be obtained as:

$$\begin{cases} 2\pi J_p \omega_g sf + 2\pi D_p \delta f = P_{rf} - P \\ J_q s E_M = Q_{rf} - Q \end{cases} \tag{4}$$

By combining (2) with (3), the coupling relationship among active-, reactive-power, *frequency*, and voltage magnitude is expressed by linearizing the equation at equilibrium point, i.e.,

$$\begin{bmatrix} \Delta P \\ \Delta Q \end{bmatrix} = \begin{bmatrix} h_{fp} & h_{ep} \\ h_{fq} & h_{eq} \end{bmatrix} \begin{bmatrix} \Delta\delta f \\ \Delta\delta E \end{bmatrix} \tag{5}$$

where h_{fp}, h_{ep}, h_{fq}, h_{eq} are the coupling factors among active- and reactive-power with frequency and voltage magnitude of VSG.

B. Open-Loop System Model (OLSM) for frequency-voltage induced-stability

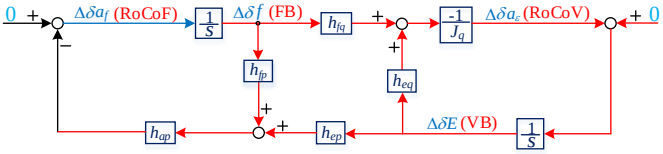

Fig. 3 Closed-loop magnitude-phase framework of GFM-VSG system

As shown in (5), $\Delta\delta f$ and $\Delta\delta E$ represent the FB and voltage magnitude bias of the VSG. Thus, the rate of change of frequency (RoCoF) and rate of change of voltage (RoCoV) can be derived as:

$$\begin{cases} \Delta\delta a_f = \frac{d\Delta\delta f}{dt} = s\Delta\delta f \\ \Delta\delta a_\varepsilon = \frac{d\Delta\delta E}{dt} = s\Delta\delta E \end{cases} \tag{6}$$

It is seen in (6) that once the RoCoF and RoCoV is generated, the FB and voltage bias (VB) naturally appears over time. Here the frequency acceleration and voltage acceleration is defined to clarify the rate of change since that the analogy can be shown in Table II with comparison between SG and VSG.

TABLE II. Analogy of Physical Characteristics Between SG and VSG

Index / Category	Moment of Inertia	Kinetic Energy	Acceleration	Velocity

SG	J (rotor)	$0.5J\omega_r^2$	$d\omega_r/dt$	$\delta\omega_r$
VSG	J_p (virtual rotor)	$0.5J_p\omega^2$	$d\omega/dt$	$\delta\omega$

Combining (4), (5) with (6), an OLSM can be obtained as shown in Fig. 3, where the dynamic interactive behavior among RoCoF, RoCoV, FB and VB can be judged. By disassembling Fig. 3, ten coupling feedback frameworks by relating RoCoF and FB with RoCoV and VB can be derived.

In general, the variables within the OLSM can be categorized into two types, i.e., active-power channel and reactive-power channel. The former one mainly includes the variables, like RoCoF, FB, and phase angle. And the latter one mainly contains the variables of RoCoV and VB. The OLSM can be used for clarifying the interaction between frequency and voltage or between RoCoF and RoCoV. This interactive phenomenon can be regarded as the *induced-stability* phenomenon.

Set the *Type* I in OLSM as an example, the state of RoCoF at the i^{th} moment impose effect on the state of RoCoV at the i^{th} moment through the coupling dynamics, then RoCoV$^{(i)}$ in turn imposes impact on RoCoF at the $(i+1)^{th}$ moment.

Thus, the RoCoF at next moment can be judged by the proposed OLSM model. This dynamic process can be also interpreted as that RoCoF at the i^{th} moment interacts with the RoCoF at the $(i+1)^{th}$ moment through the middle variable (RoCoV$^{(i)}$ in this example). It was defined as the *induced-stability*, because dynamics of RoCoF is influenced by the middle variable in the *other channel*, which in turn impacts RoCoF.

Similarly, the other nine coupling feedback frameworks have similar characteristics. Therefore, the transfer function from state at the i^{th} moment to the state at the $(i+1)^{th}$ moment in ten feedback frameworks can be derived as:

$$\text{Type I: } \frac{\Delta\delta a_f{}^{(i+1)}}{\Delta\delta a_f{}^{(i)}} = \frac{\Delta\delta a_\varepsilon{}^{(i)}}{\Delta\delta a_f{}^{(i)}}\frac{\Delta\delta a_f{}^{(i+1)}}{\Delta\delta a_\varepsilon{}^{(i)}} = F_{avf}(s)G_{afv}(s) \quad (7)$$

$$\text{Type III: } \frac{\Delta\delta a_\varepsilon{}^{(i+1)}}{\Delta\delta a_\varepsilon{}^{(i)}} = \frac{\Delta\delta\theta^{(i)}}{\Delta\delta a_\varepsilon{}^{(i)}}\frac{\Delta\delta a_\varepsilon{}^{(i+1)}}{\Delta\delta\theta^{(i)}} = F_{thv}(s)G_{vth}(s) \quad (8)$$

$$\text{Type V: } \frac{\Delta\delta a_\varepsilon{}^{(i+1)}}{\Delta\delta a_\varepsilon{}^{(i)}} = \frac{\Delta\delta f^{(i)}}{\Delta\delta a_\varepsilon{}^{(i)}}\frac{\Delta\delta a_\varepsilon{}^{(i+1)}}{\Delta\delta f^{(i)}} = F_{fav}(s)G_{avf}(s) \quad (9)$$

$$\text{Type VII: } \frac{\Delta\delta a_f{}^{(i+1)}}{\Delta\delta a_f{}^{(i)}} = \frac{\Delta\delta E^{(i)}}{\Delta\delta a_f{}^{(i)}}\frac{\Delta\delta a_f{}^{(i+1)}}{\Delta\delta E^{(i)}} = F_{eaf}(s)G_{afe}(s) \quad (10)$$

$$\text{Type IV: } \frac{\Delta\delta f^{(i+1)}}{\Delta\delta f^{(i)}} = \frac{\Delta\delta E^{(i)}}{\Delta\delta f^{(i)}}\frac{\Delta\delta f^{(i+1)}}{\Delta\delta E^{(i)}} = F_{vf}(s)G_{fv}(s) \quad (11)$$

where ten feedback frameworks are signed with type I to type X according to the sequence in Fig. 4. It was found in Fig. 4 that the transfer functions of *Type* II, IV, VI, VIII and X are the same as that of *Type* I, III, V, VII, IX according to the duality principle of the circuit theory.

It reflects the phenomenon that the variables in active-power channel (or in reactive-power channel) interact with the reactive-power channel (or active-power channel) through RoCoF-RoCoV coupling dynamics, and in turn impose effect on itself. Thus, this phenomenon is defined as *induced-stability*.

It can be found that the derived functions in Type I, III, V, VII, IX are the same, which satisfies:

$$F_{avf}(s)G_{afv}(s) = F_{thv}(s)G_{vth}(s) = F_{fav}(s)G_{avf}(s) = F_{eaf}(s)G_{afe}(s) = F_{vf}(s)G_{fv}(s) \quad (12)$$

Therefore, they have common transfer functions from Type I to Type X. Naturally, a unified OLSM model is proposed to judge the *induced-stability* of the system, i.e.,

$$\frac{\Delta x^{(i+1)}}{\Delta x^{(i)}} = \frac{\Delta y^{(i)}}{\Delta x^{(i)}}\frac{\Delta x^{(i+1)}}{\Delta y^{(i)}} = F(s)G(s) \quad (13)$$

According to the symmetry and duality principle, (13) can be rearranged as:

$$\frac{\Delta y^{(i+1)}}{\Delta y^{(i)}} = \frac{\Delta x^{(i)}}{\Delta y^{(i)}}\frac{\Delta y^{(i+1)}}{\Delta x^{(i)}} \quad (14)$$

where $\Delta x^{(i+1)}$ and $\Delta x^{(i)}$ represent anyone of variables in active-power channel at the $(i+1)^{(th)}$ moment and at the $i^{(th)}$ moment.

The ***induced-stability*** can be interpreted by the impact of $\Delta x^{(i)}$ on the dynamics of $\Delta y^{(i)}$ that in turn feedback to the dynamics of the $(i+1)^{(th)}$ moment $\Delta x^{(i+1)}$.

It should be noted that OLSM is different from the conventional Open-Loop control system which identifies the magnitude-margin and phase-margin of the closed-loop system. This generic OLSM (Eq. (13) and (14)) can judge the *induced-stability* as well as the dynamic property of the system. The identification procedure of OLSM was found in Fig. 5(a).

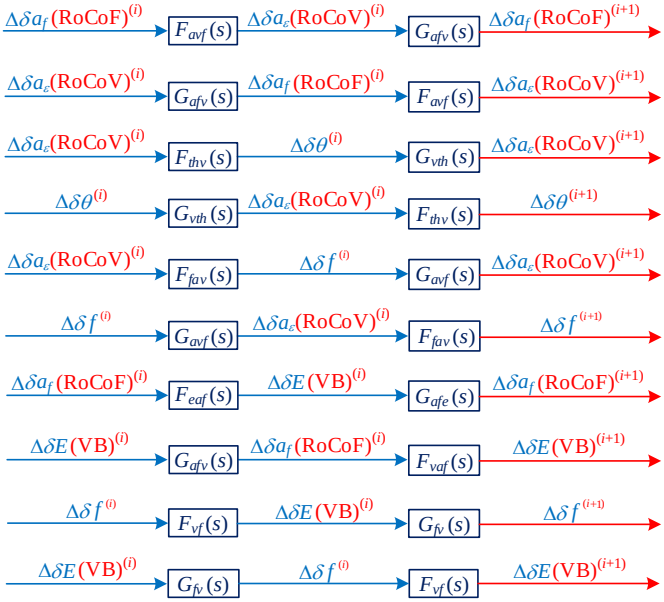

Fig. 4 The OLSM for *induced-stability* of frequency-voltage in GFM-VSG system: ten channels

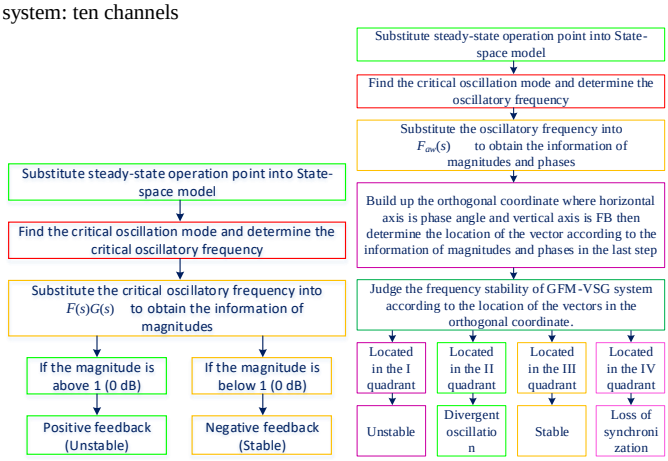

Fig. 5 Flowchart of procedure, (a) *induced-stability* identification by the OLSM (Δx goes to the variable in active-power channel and Δy goes to the variable in reactive-power channel), (b) frequency/voltage stability by the MPFAM

C. Magnitude-phase feedback analytical model (MPFAM) based on frequency self-stability

In Section II-Part B, *induced-stability*, characterized by the interaction between voltage and frequency, was discussed by the proposed OLSM. In this part, the frequency self-stability is studied by the proposed MPFAM, which belongs to the internal coupling between RoCoF and FB.

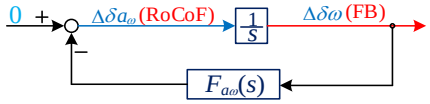

Fig. 6 MPFAM for self-stability of frequency in GFM-VSG system [14]

There naturally exist the integral relationship between RoCoF and FB, thus this type of stability is defined as self-stability of frequency in GFM-VSG system, as evidenced by Fig. 6.

Distinct from the generic OLSM for *induced-stability* criterion, this MPFAM is used for self-stability analysis of frequency. Specifically, this MPFAM is used for internal-feedback behavior evaluation from FB to RoCoF. Another distinction between two analytical methods lies in that the former one is essentially an Open-Loop system, but the latter one is Closed-Loop system.

Fig. 5(b) displays the identification procedure of self-stability analysis with the MPFAM, with which the oscillation-stability and loss of synchronization-stability in frequency of GFM-VSG system can be evaluated.

D. Validation of the proposed model

With linearization, the small-signal state-space representation can be derived as:

$$\frac{d\Delta x}{dt} = A\Delta x + B\Delta u \tag{15}$$

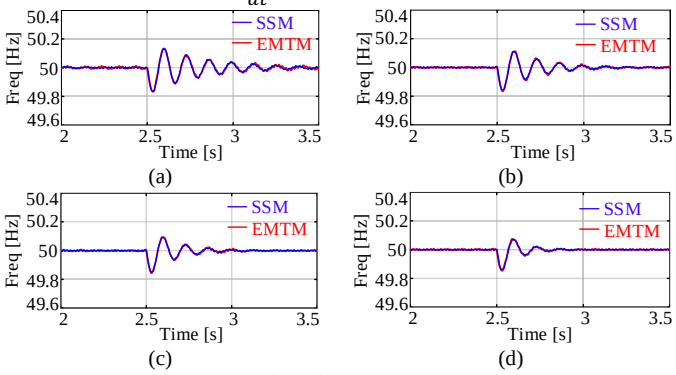

Fig. 7 Time-domain response of the frequency subjected to power disturbance with small-signal model (SSM) and electromagnetic transient model (EMTM)

where Δx is the state variable, Δu denotes the input variable. The letter A and B represent the state-matrix and input-matrix. Each state-variable and input-variable is given as:

$$\begin{cases} \Delta x = [\Delta I_d, \Delta I_q, \Delta\delta\theta, \Delta\delta f, \Delta\delta E]^T \\ \Delta u = [\Delta P_{rf}, \Delta Q_{rf}, \Delta f_G, \Delta U_G]^T \end{cases} \tag{16}$$

where Δf_G *and* ΔU_G are grid frequency and voltage magnitude. ΔI_d and ΔI_q are the components reflected in the rotational synchronous inertia coordinates. $\Delta\delta\theta, \Delta\delta f, \Delta\delta E$ represent the angle deviation, frequency deviation and the voltage deviation.

And $$\begin{cases} I_d = I_g cos\delta\varphi_i \\ I_q = I_g sin\delta\varphi_i \end{cases}$$

Fig. 7 shows the frequency response subjected to power disturbance by comparing SSM with EMTM. The EMTM is developed by electromagnetic switching model and SSM is developed by the average small signal model. It can be seen that two responses are highly matched, which verifies the effectiveness and accuracy of the proposed model.

III. Stability Analysis and Origin of Oscillation

A. Stability analysis of GFM-VSG system by OLSMM

In this part, the stability analysis of GFM-VSG system is developed by the proposed OLSM to illustrate the mechanism of *induced-stability* with RoCoF/RoCoV.

Here the principle of OLSM is briefly introduced. In reality, the OLSM in (13) and (14) are essentially the same due to the symmetry and duality principle. Thus, set (13) as an example to clarify the principle.

$$\Delta x^{(i+1)} = \tau\Delta x^{(i)} \tag{17}$$

where $$\tau = \|F(s)G(s)\|_{\omega=\omega_{cf}} = 10^{\frac{M}{20}}$$

where τ is a physical quantity that reflects the speed of monotonic increase or monotonic decrease whatever for oscillation-stability or loss of synchronization-stability. ω_{cf} goes to critical frequency. '|| ||' signifies the absolute value of the transfer function. M denotes the magnitude of the transfer function at ω_{cf} with the unit of Decibel (dB).

Given that oscillation can be considered as a periodic fluctuation of RoCoF/FB or RoCoV/VB, thus ω_{cf} can reflect the periodicity since that it is the 'reciprocal of period'.

Eq. (17) can be rearranged as:

$$\frac{\Delta x^{(i+1)}}{\Delta t} = \tau\frac{\Delta x^{(i)}}{\Delta t} \to \lim_{\Delta t\to 0}\frac{dx^{(i+1)}}{dt} = \tau\lim_{\Delta t\to 0}\frac{dx^{(i)}}{dt} \tag{18}$$

It can be inferred from (18) that Δx will go to infinite divergence if $\tau > 1$ is satisfied, which forms a positive feedback effect (PFE). Nevertheless, Δx will go to convergence if $\tau < 1$ is satisfied, which forms a negative feedback effect (NFE). In this Case, the smaller τ indicates stronger NFE while larger τ suggests weaker NFE. It means that τ will impose effect on motion trajectory of RoCoF/FB/RoCoV/VB.

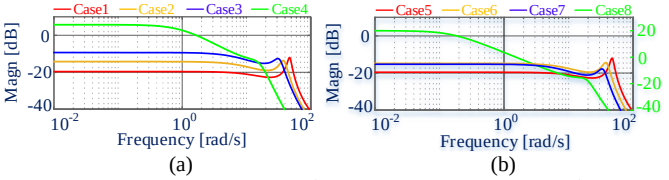

Fig. 8 Frequency responses curves of $F(s)G(s)$, (a) the same ratio of resistance divided by inductance of grid (L_G/R_G), (b) different ratio of L_G/R_G

The parameters of L_G/R_G from case 1 to case 8 are presented in Table III. It was seen the ratio of L_G/R_G is fixed from Case 1 to Case 4. This is to certificate the impact of grid-strength on OS and LoSS under the same ratio of L_G/R_G. However, L_G/R_G is variable with the fixed grid resistance from Case 5 to Case 8.

TABLE III. PARAMETERS OF L_G/R_G FROM CASE 1 TO CASE 8

	L_G	R_G
Case 1	6.6 mH	0.15 Ω
Case 2	11 mH	0.25 Ω
Case 3	15.4 mH	0.35 Ω
Case 4	20.9 mH	0.45 Ω
Case 5	6.6 mH	0.15 Ω
Case 6	11 mH	0.15 Ω
Case 7	15.4 mH	0.15 Ω
Case 8	20.9 mH	0.15 Ω

Table IV shows the *key* information originated from the frequency response curves in Fig. 8 that relationship among feedforward coefficient τ, oscillation frequency of theoretical

value, oscillation frequency of simulation value (see simulations) and the operation conditions is presented.

Grid-strength is defined by the reciprocal of the grid impedance [17], i.e.,

$$k_{str} = \frac{1}{\left(\sqrt{{R_G}^2+(\omega_0 L_G)^2}\right)^*} \tag{19}$$

TABLE IV. PARAMETERS OF L_G/R_G FROM CASE 1 TO CASE 8

	τ	Theoretical	Simulation
Case 1	0.2512	7.464 Hz	7.557 Hz
Case 2	0.2089	6.1275 Hz	6.218 Hz
Case 3	0.2344	5.109 Hz	5.186 Hz
Case 4	1.9364	0 Hz	0 Hz
Case 5	0.2512	7.464 Hz	7.557 Hz
Case 6	0.1905	6.08 Hz	6.139 Hz
Case 7	0.1288	5.188 Hz	5.181 Hz
Case 8	9.8855	0 Hz	0 Hz

It can be seen that critical oscillation frequency (COF) gets declined as grid-strength is decreased with the same ratio of L_G/R_G (See from Case 1 to Case 4). However, the feedforward coefficient τ is not monotonically decreased as grid-strength is decreased. It may be due to the fact that the grid resistance also imposes effect on attenuation of OS. It can be also inferred that GFM-VSG can operate stably in weak grid condition [12]. From Table IV, it was also found that the theoretical value of oscillation frequency is nearly coincident with simulated value.

It can be seen that $\tau = 1.9364$ and oscillation frequency is zero if L_G=20.9 mH and R_G=0.45 Ω. It illustrates that system has a risk of loss of synchronism in the weaker grid condition. Nevertheless, ultra-weak condition is not normally occurring in the real power grid operation and even it can be avoided during the stage of grid-planning or grid-dispatching, which is more likely a planning and dispatching problem.

As seen from Case 5 to Case 7, both feedforward coefficient τ and COF are declined as grid-strength gets weaker. It certificates that both damping performance and inertia level gets better and higher as grid-strength gets weaker within certain ranges. This analytical result shows that VSG owns superior performance as it is attached to weak power network.

However, $\tau = 9.8855$ and COF is 0 Hz if L_G=20.9 mH and R_G=0.15 Ω. In this case, VSG loses synchronization with power network, and frequency deviates from nominal value in a manner of PFE. It is seen that Case 8 has triple ratio of L_G/R_G higher than that of Case 4, and thus feedforward coefficient τ is much higher in Case 8, which suggests that higher ratio of L_G/R_G and higher L_G value can cause higher risk of loss of synchronization. However, this risk can be avoided if the design of grid-strength is planned in the constraint condition during the stage of grid-planning and grid-dispatching, which stands at a higher level and more macroscopic altitude. Normally the ultra-weak grid condition is unusual in the real engineering.

In general, both grid-strength and ratio of L_G/R_G will influence the damping performance and inertia level of GFM-VSG system since that speed of oscillation attenuation becomes faster and COF gets slower as grid-strength gets weaker. The speed of oscillation attenuation can reflect the damping level of the system, i.e., the faster speed is, the larger damping level is. Besides, the COF can reflect the inertia level as the inertia aims to impede the further change of the variable and thus leaves it much slower. The slower COF means the slower RoCoF and the smoother change of frequency. Nevertheless, this change law is within certain ranges of change of grid-strength. When the grid-strength gets weaker (e.g., Case 4 and 8), VSG has the higher risk of loss of synchronism with power network. This phenomenon is illustrated by that COF declines and approaches to 0 Hz as grid-strength gets weaker. Nevertheless, the ultra-weak condition can be avoided as long as the design of the grid strength is considered in the stage of grid-planning or grid-dispatching.

In general, the conclusions on relationship between grid strength and stability derived by the OLSM method can be summarized as follows:

- In fact, the extent of the 'weak' with weak grid is comparatively/relatively where there is no strict and absolute boundary between weak-grid and ultra-weak-grid since that weak is relative instead of absolute.
- From another dimension, the 'weak' also means that the VSG in grid-forming mode can operate more stably and provide better frequency and voltage support capability than that in grid-following mode. Besides, this characteristic is reflected more obvious especially when grid strength gets weaker that the grid-following converter is more prone to loss of stability than that of grid-forming VSG.

B. Self-stability analysis of GFM-VSG system for frequency dynamics by MPFAM

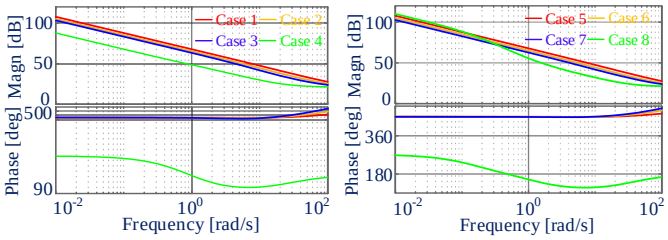

Fig. 9 Frequency responses of $F_{a\omega}(s)$, (a) $F_{a\omega}(s)$ with Case 1 to Case 4, (b) $F_{a\omega}(s)$ with Case 5 to Case 8

TABLE V. MAGNITUDE, PHASE AND COF OF $F_{a\omega}(s)$

	Magn	Phase	COF
Case 1	33.9 dB	96 deg	7.464 Hz
Case 2	32.3 dB	101 deg	6.1275 Hz
Case 3	31.1 dB	104 deg	5.109 Hz
Case 4	87.8 dB	-92 deg	0 Hz
Case 5	33.9 dB	96 deg	7.464 Hz
Case 6	32.3 dB	101 deg	6.08 Hz
Case 7	31.5 dB	104 deg	5.188 Hz
Case 8	130 dB	-91 deg	0 Hz

Table V shows the information of magnitude, phase and COF of $F_{a\omega}(s)$ from Fig. 9. Then, the location of the vectors is determined according to the information, as shown in Fig. 10.

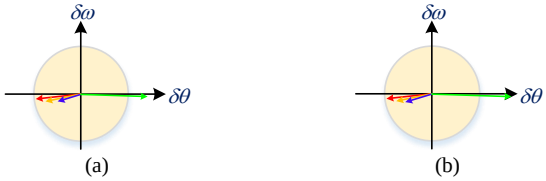

Fig. 10 Vector diagram analysis by MPFAM, (a) Case 1 to Case 4, (b) Case 5 to Case 8

Fig. 10(a) shows that vectors are located in the third quadrant, which indicates that the frequency is convergence to equilibrium point with attenuated oscillation. In addition, attenuation speed is faster as grid-strength gets weaker within a

certain ranges because the vertical component of the vector is more negative versus to $\delta\omega$-axis. However, the horizontal component is less negative to $\delta\theta$-axis which indicates that the synchronization ability gets weaker as grid-strength becomes weaker.

It even loses synchronization with the weaker power network in Case 4, as can be shown in the green arrow. The green arrow indicates a PFE that the disturbance will increase the angle continuously. The similar phenomena occur in Case 5 to 8, thus here it is no longer illustrated.

C. Origin analysis of oscillation in GFM-VSG system

In this part, the origin of frequency oscillation is clarified by the equivalent second-order model of MPFAM in GFM-VSG system. Besides, a qualitative analysis is carried out from perspective of ***inertia*** to clarify the origin of the oscillation. The analysis in Section-III-B shows that the vector can be decomposed into horizontal- and vertical-direction at the COF.

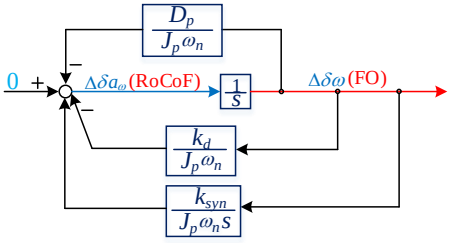

Fig. 11 Equivalent second-order model of MPFAM by rearranging Fig. 6

Thus, Fig. 6 can be rearranged as Fig. 11 by decomposition of $F_{a\omega}(s)$. k_d and k_{syn} denote the damping-component and synchronizing-component at COF. Therefore, the equivalent damping and natural oscillatory frequency are obtained by leaving the denominator of the closed-loop system equal to standard second-order model:

$$\begin{cases} \xi = \frac{D_p+k_d}{2\sqrt{J_p\omega_n k_{syn}}} \\ \omega_{cf} = \sqrt{\frac{k_{syn}}{J_p\omega_n}} \end{cases} \tag{20}$$

Several conclusions can be drawn from (20), i.e., larger synchronizing-component causes higher COF, which means that stronger grid-strength leads to higher COF. It was inferred from Table IV that the COF is equal to zero when grid-strength is weaker. In addition, larger virtual inertia leads to lower COF. Stronger grid-strength causes poorer damping performance, of which the phenomenon is consistent with that stronger grid-strength leads to higher COF.

According to (20), VSG frequency is derived as:

$$f(t) = e^{-\frac{D_p+k_d}{2J_p\omega_n}t}\sin\left(\frac{\sqrt{4J_p\omega_n k_{syn}-(D_p+k_d)^2}}{2J_p\omega_n}t+\varphi\right) \tag{21}$$

By differentiating (19), RoCoF is derived as:

$$\frac{df(t)}{dt} = \sqrt{\frac{k_{syn}}{J_p\omega_n}}e^{-\frac{D_p+k_d}{2J_p\omega_n}t}\sin\left(\frac{\sqrt{4J_p\omega_n k_{syn}-(D_p+k_d)^2}}{2J_p\omega_n}t+\varphi+\theta_{bias}\right) \tag{22}$$

where $\theta_{bias} = \arctan[(D_p+k_d) - \frac{4J_p\omega_n k_{syn}}{(D_p+k_d)}]$

By comparing (22) with (21), it is inferred that there exists a phase angle bias between RoCoF and the frequency, which is the radical origin of the oscillation. It was because that any non-zero RoCoF suggests imbalanced active-power, and thus RoCoF and the frequency cannot synchronize and reach zero simultaneously due to the phase angle bias. Condition $\theta_{bias} = 0$ is satisfied if and only if the following condition is held:

$$D_p + k_d = 2\sqrt{J_p\omega_n k_{syn}} \tag{23}$$

Substituting (23) into (20), the damping ratio is justly equal to 1, which means there is no overshoot and oscillation. It further consolidates the deduction.

From another perspective, inertia always leaves the VSG frequency maintaining the initial operation state and thus do not abruptly change, on the other side, damping aims to impede the further motion of frequency. Thus, it can be controversial to see this phenomenon that the inertia, damping and stiffness can impact the oscillation but they are all the radical origin of the oscillation, as evidenced by (22) and (23).

From another view, k_d and k_{syn} is derived when the COF is substituted into $F_{a\omega}(s)$. That is to say, the prerequisite of k_d and k_{syn} is the generated COF, which will at least trigger attenuated oscillation as long as COF is not zero.

Provided that virtual inertia increases, and J_p is increased to the larger J_p', then the increment of virtual inertia can lead to equivalent change of damping and stiffness, as inferred from Fig. 11. The variation of damping and inertia are derived as:

$$\begin{cases} \delta D_p = -\frac{D_p+k_d}{J_pJ_p'\omega_n}\delta J_p \\ \delta k_{syn} = -\frac{k_{syn}}{J_pJ_p'\omega_n}\delta J_p \end{cases} \tag{24}$$

where $\delta J_p = J_p' - J_p$

It can be inferred that inertia is coupled with damping and stiffness of the GFM-VSG system. In addition, the increment of virtual inertia leads to decline of damping and stiffness.

IV. Simulations and Experiments

A. Simulations

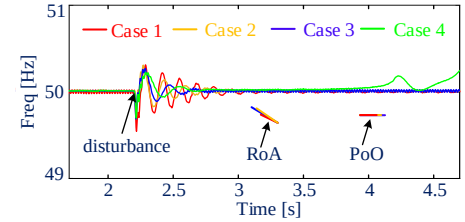

(a)

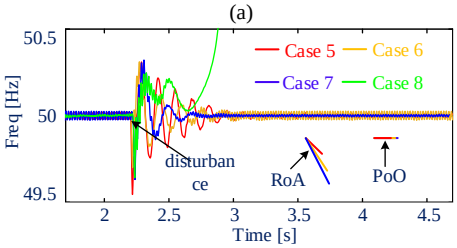

(b)

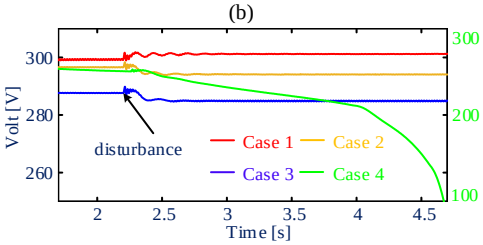

(c)

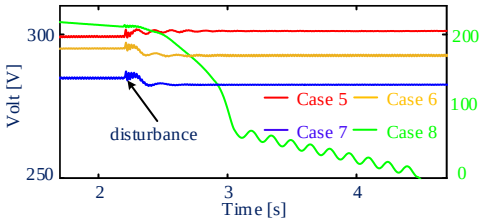

(d)

Fig. 12 Simulation results of Frequency and Voltage in GFM-VSG system, (a) Frequency from Case 1 to Case 4, (b) Frequency from Case 5 to Case 8, (c) Voltage magnitude from Case 1 to Case 4, (d) Voltage magnitude from Case 5 to Case 8

This part gives the simulation results to demonstrate the effectiveness of proposed modeling and analytical method. The parameters of VSG control and *L*-filter except for grid-impedance (See Table III) are provided here: J_p=0.057, D_p=235.6, J_q=10, R_F=0.1 Ω, L_F=4.4 mH.

It shows that RoCoF gets slower and FB gets smaller during post-disturbance as grid-strength gets weaker (Case 1 to Case 3). Also, the attenuation speed gets slower as grid-strength gets weaker within a certain range. However, VSG lose synchronization with power network and frequency deviates from nominal value in a manner of aperiodic LoS. Simulation phenomena are consistent with theoretical analysis by OLSM and MPFAM. The voltage has the similar dynamics with that of frequency, which consolidates the effectiveness of OLSM.

Fig. 12(b) and (d) shows the frequency and voltage magnitude with Case 5 to Case 8. RoCoF and FB are slower and smaller as grid-strength gets weaker. However, when it comes to Case 8, VSG cannot synchronize with power network in the weaker grid-strength. Although this loss of synchronism is aggravate the secure operation of the system, it can be avoided if the unexpected grid-strength is planned in the constraint condition during the stage of grid-planning or grid-dispatching.

B. Experiments

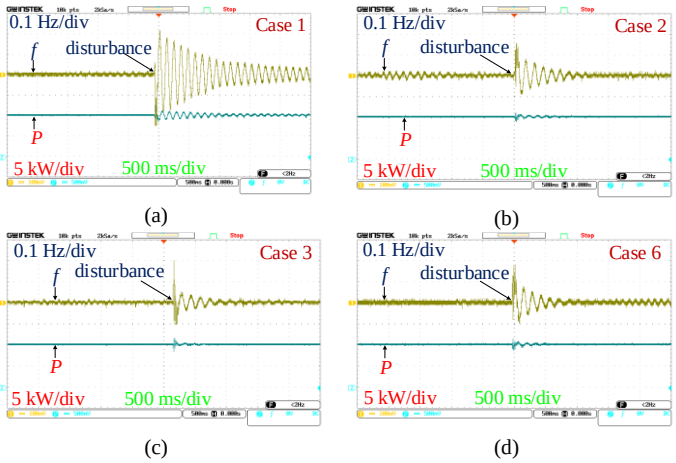

Fig. 13 Experimental results of frequency and active-power, (a) Case 1, (b) Case 2, (c) Case 3, (d) Case 6

The experiments are developed according to the topology and control strategy in Fig. 2, where the system parameters are as the same as that of simulations in Case 1, 2, 3, and 6. Note that the FB and real active-power are collected to show experiments results.

As can be seen in Case 1, the maximum FB is approximately 0.22 Hz, and the frequency oscillation gets convergent. The active-power oscillates in the same manner. Compared to Case 1, the oscillation of RoCoF, FB, and active-power are smaller in Case 2, which indicates that decline of grid-strength results in better damping performance and faster attenuation speed of the oscillation. Moreover, the FB and oscillation of active-power gets smaller in Case 3 than that in Case 2, further demonstrating the law. By comparing Case 6 with Case 2, the attenuation speed is faster in Case 6 than Case 2 since inductances are the same but ratio of L/R is higher in Case 6. Therefore, the experiments are well matched with the theoretical analysis, validating the effectiveness of the proposed modeling.

V. Conclusions

This work explored the investigation on the physical insight into frequency and voltage stability in grid-forming virtual synchronous generator (GFM-VSG) system. A generic Open-Loop System Model (OLSM) was proposed to accurately analyze the mechanism of frequency-voltage induced-stability, the internal interaction mechanism between rate of change of frequency (RoCoF) and rate of change of voltage (RoCoV) was established. In addition, the frequency self-stability was evaluated by proposed magnitude-phase feedback analytical model (MPFAM). Following conclusions were drawn:

(1) It was found that the low-frequency oscillation (LFO) analysis between OLSM and MPFAM analytical frameworks have the same conclusions in the same conditions. It can be inferred that the LFO between frequency and voltage magnitude are coupled, of which the characteristic does not resemble with the frequency/voltage stability in conventional synchronous generator-dominated power system.

(2) It was found that GFM-VSG can operate stably in weak power network but cannot operate well in ultra-strong power network. And there is a high risk of LFO when it is connected to ultra-strong power network. This characteristic is different from that of grid-following inverter system.

(3) LFO mechanism of GFM-VSG system was clarified from perspective of ***inertia***. Due to inertia property of the system, RoCoF cannot maintain synchronization with frequency bias. Therefore, the LFO is inevitable. In addition, the physical essence of the self-stability and *induced-stability* as well as ***oscillation propagation*** was clearly clarified, which sketched a new perspective for the dynamic property in GFM-VSG.

Besides of conclusions, a distinction between two analytical methods lies in that the former one is essentially an Open-Loop System, but the latter one is Closed-Loop System. The Open-Loop System can identify the dynamic property of the system, which filled up with the gaps of the conventional Open-Loop control system. However, the conclusion can be drawn that frequency is coupled with voltage magnitude according to the two criteria.

Acknowledgements

This work was supported by the State Grid Corporation Headquarters Management Technology Project: Operation Characteristics and Stability Control of Universal Active Support Power Electronic Equipment Power System (52120522003P).

REFERENCES

[1] K. R. Vasudevan, V. K. Ramachandaramurthy, T. S. Babu and A. Pouryekta, "Synchronverter: A Comprehensive Review of Modifications, Stability Assessment, Applications and Future Perspectives," in *IEEE Access*, vol. 8, pp. 131565-131589, 2020.

[2] M. Pourmohammad, M. Toulabi and A. M. Ranjbar, "Application of State Feedback Controller to Ensure Robust D-Stable Operation of Virtual Synchronous Generators," in *IEEE Transactions on Energy Conversion*, vol. 36, no. 2, pp. 602-610, June 2021.

[3] J. Rold án-P érez, A. Rodr íguez-Cabero and M. Prodanovic, "Design and Analysis of Virtual Synchronous Machines in Inductive and Resistive Weak Grids," in *IEEE Transactions on Energy Conversion*, vol. 34, no. 4, pp. 1818-1828, Dec. 2019.

[4] J. M. Mauricio and A. E. Leon, "Improving Small-Signal Stability of Power Systems With Significant Converter-Interfaced Generation," in *IEEE Transactions on Power Systems*, vol. 35, no. 4, pp. 2904-2914, July 2020.

[5] H. Liu, D. Sun, P. Song, X. Cheng, F. Zhao and Y. Tian, "Influence of Virtual Synchronous Generators on Low Frequency Oscillations," in *CSEE Journal of Power and Energy Systems*, vol. 8, no. 4, pp. 1029-1038, July 2022.

[6] W. Du, Q. Fu and H. F. Wang, "Power System Small-Signal Angular Stability Affected by Virtual Synchronous Generators," in *IEEE Transactions on Power Systems*, vol. 34, no. 4, pp. 3209-3219, July 2019.

[7] H. Zhang *et al*., "Comparison of Low Frequency Oscillation Characteristic Differences between VSG and SG," *2020 IEEE Sustainable Power and Energy Conference (iSPEC)*, Chengdu, China, 2020, pp. 668-673.

[8] G. Wang, L. Fu, Q. Hu, F. Ma, C. Liu and Y. Lin, "Low Frequency Oscillation Analysis of VSG Grid-Connected System," *2021 3rd Asia Energy and Electrical Engineering Symposium (AEEES)*, Chengdu, China, 2021, pp. 631-637.

[9] Y. Liu, X. Zhou, Y. Chen, L. Zhou, L. Wang and W. Wu, "Sequence Impedance Modeling and Stability Analysis for Load Converters With Inertial Support," in *IEEE Transactions on Power Electronics*, vol. 35, no. 12, pp. 13031-13041, Dec. 2020.

[10] Y. Yu, M. Zhang, M. Antoine and H. Li, "Analysis of Synchronous Frequency Resonance in VSG Based on the Sequence Impedance Models," *2019 22nd International Conference on Electrical Machines and Systems (ICEMS)*, Harbin, China, 2019, pp. 1-6.

[11] N. Dong, H. Yang and J. Han, "Small-Signal Modeling and Impedance Analysis of Virtual Synchronous Generator," *2018 IEEE International Power Electronics and Application Conference and Exposition (PEAC)*, Shenzhen, China, 2018, pp. 1-6.

[12] C. Li *et al*., "Generalized Stabilizer-Oriented Design for GFVSG Integrated Into Weak-Stiffness Power Networks," in *IEEE Transactions on Power Systems*, vol. 37, no. 6, pp. 4958-4961, Nov. 2022.

[13] C. Li, Y. Yang, N. Mijatovic and T. Dragicevic, "Frequency Stability Assessment of Grid-Forming VSG in Framework of MPME With Feedforward Decoupling Control Strategy," in *IEEE Transactions on Industrial Electronics*, vol. 69, no. 7, pp. 6903-6913, July 2022.

[14] C. Li *et al*., "New Framework of RoCoF-FD for Wideband Stability Evaluation in Renewable Energy Generators With Virtual Impedance Control," in *IEEE Transactions on Smart Grid*, vol. 13, no. 5, pp. 3570-3581, Sept. 2022.

[15] C. Li, Y. Yang, Y. Cao, L. Wang and F. Blaabjerg, "Frequency and Voltage Stability Analysis of Grid-Forming Virtual Synchronous Generator Attached to Weak Grid," in *IEEE Journal of Emerging and Selected Topics in Power Electronics*, vol. 10, no. 3, pp. 2662-2671, June 2022.

[16] M. Farrokhabadi *et al*., "Microgrid Stability Definitions, Analysis, and Examples," in *IEEE Transactions on Power Systems*, vol. 35, no. 1, pp. 13-29, Jan. 2020.

[17] N. Hatziargyriou *et al*., "Definition and Classification of Power System Stability – Revisited & Extended," in *IEEE Transactions on Power Systems*, vol. 36, no. 4, pp. 3271-3281, July 2021.

Chang Li obtained his bachelor degree in 2014 at Guizhou University, and obtained PhD degree in July 2020 at Hunan University. After his graduation of PhD career, he began his postdoc scientific work at Technical University of Denmark until October 2021. He was also a guest Senior Lecturer from September 2021 to December 2021 and from April 2022 to October 2022 at Peter the Great Saint Petersburg Polytechnic University. Since December 2021, he began his Postdoctoral Fellow career at Hong Kong Polytechnic University. Also, he was a Research Fellow at Nanyang Technological University before joining Hefei University of Technology. He is currently an Associate Professor at Hefei University of Technology. His research interests include but not limited to modeling, analysis and control of power electronics interfaced power systems.

Yong Li (Senior Member, IEEE) received the B.Sc. and Ph.D. degrees from the College of Electrical and Information Engineering, Hunan University, Changsha, China, in 2004 and 2011, respectively. He is currently a Full Professor of electrical engineering with Hunan University. His current research interests include power system stability analysis and control, ac/dc energy conversion systems and equipment, analysis and control of power quality, and HVDC and FACTS technologies.

Yan Du received the B.Sc. degree in automatic engineering, and the MSc. and Ph.D. degrees in power electronics and power drives from the Hefei University of Technology, Hefei, China, in 2000, 2004, and 2013, respectively. She is currently an Assistant Professor with the School of Electrical Engineering and Automation, Hefei University of Technology. Her current research interests include distributed generation and micro grid control.

Xingle Gao received the B.Eng. degree in electrical engineering from North China University of Science and Technology, Tangshan, China, in 2015, and the M.Eng. degree in control science and engineering from Beijing University of Technology, Beijing, China, in 2018, and the Ph.D. degree in electrical engineering from Hunan University, Changsha, China, in 2022. He is currently an engineer with Economic Research Institute of State Grid Hebei Electric Power Co., Ltd, Shijiazhuang, China. His research interests include the modeling of electrical networks, and applications of complex networks in the assessment of robustness of power systems and cyber-physical systems.

Yaqian Yang received the Master degree in Electrical Engineering from the Changsha University of Science and Technology in 2018. and the Ph.D. degree in electrical engineering from Hunan University, Changsha, China, in 2022. She is currently an associate professor with the department of electrical engineering, Anhui Agricultural University, Hefei, China. Her current research interests include: stabilization and control of grid-forming virtual synchronous generators, synthetic inertial applied in hybrid AC/DC microgrids.

Yijia Cao (Fellow, IEEE) was born in Hunan, China, in 1969. He received the B.S. degree in applied mathematics from Xi'an Jiaotong University, Xi'an, China, in 1988, and the M.Sc. degree in applied mathematics and Ph.D. degrees in electrical engineering from the Huazhong University of Science and Technology (HUST), Wuhan, China, in 1991 and 1994, respectively. From 1994 to 2000, he was a Visiting Research Fellow and a Research Fellow with

Loughborough University, Liverpool University, and the University of the West England, U.K. From 2000 to 2001, he was a Full Professor with HUST, and from 2001 to 2008, he was a Full Professor with Zhejiang University, and from 2008 to 2018, he was a Full Professor with Hunan University, China. In 2008, he was the Vice President of Hunan University. He is currently a Full Professor and the President of the Changsha University of Science and Technology, Changsha, China. His research interests include power system stability control and the application of intelligent systems in power systems.

Frede Blaabjerg (S'86–M'88–SM'97–F'03) was with ABB-Scandia, Randers, Denmark, from 1987 to 1988. From 1988 to 1992, he got the PhD degree in Electrical Engineering at Aalborg University in 1995. He became an Assistant Professor in 1992, an Associate Professor in 1996, and a Full Professor of power electronics and drives in 1998. From 2017 he became a Villum Investigator. He is honoris causa at University Politehnica Timisoara (UPT), Romania and Tallinn Technical University (TTU) in Estonia.

His current research interests include power electronics and its applications such as in wind turbines, PV systems, reliability, harmonics and adjustable speed drives. He has published more than 600 journal papers in the fields of power electronics and its applications. He is the co-author of four monographs and editor of ten books in power electronics and its applications